Eur. Phys. J. A **22**, 75–87 (2004)
DOI 10.1140/epja/i2004-10030-0

THE EUROPEAN PHYSICAL JOURNAL A

The influence of the entrance channel dynamics on the evaporation residue formation

G. Fazio[1], G. Giardina[1,a], A. Lamberto[1], A.I. Muminov[2], A.K. Nasirov[2,3], F. Hanappe[4], and L. Stuttgé[5]

[1] INFN, Sezione di Catania, and Dipartimento di Fisica dell'Università di Messina, Messina, Italy
[2] Heavy Ion Physics Department, INP, Tashkent, Uzbekistan
[3] Bogoliubov Laboratory of Theoretical Physics, JINR, Dubna, Russia
[4] Université Libre de Bruxelles, Bruxelles, Belgium
[5] Institut de Recherches Subatomiques, Strasbourg, France

Received: 8 March 2004 / Revised version: 5 April 2004 /
Published online: 25 October 2004 –
Communicated by D. Guerreau

Abstract. The dynamical effects of the entrance channel on the competition between quasifission and fusion processes, and on the evaporation residue formation are investigated. We have analyzed the results and compared our calculations with the experimental data obtained in the $^{16}O + {}^{204}Pb$ and $^{96}Zr + {}^{124}Sn$ reactions having very different mass asymmetries and leading to the $^{220}Th^*$ compound nucleus. We have found that different partial capture cross-sections $\sigma_\ell^{cap}(E)$ for these reactions lead to different fusion-quasifission competitions and, consequently, to different partial fusion cross-sections $\sigma_\ell^{fus}(E)$ of the compound nucleus formed in the two reactions. The dynamical conditions also affect the fission-evaporation competition of the excited intermediate nuclei along the CN de-excitation cascade and, consequently, the evaporation residue formation.

PACS. 25.70.Jj Fusion and fusion-fission reactions – 25.70.-z Low and intermediate energy heavy-ion reactions – 27.80.+w $190 \leq A \leq 219$ – 27.90.+b $220 \leq A$

1 Introduction

The difference between measured evaporation residues (ER), obtained in reactions [1–5] having different projectile and target nucleus combinations, and leading to the same compound nucleus (CN) with charge Z and mass A, can be explained by the dependence of the partial fusion cross-section $\sigma_\ell^{fus}(E)$ and survival probability $W_{sur}(E,\ell)$ against fission of the excited CN on the peculiarities of the entrance channel. Generally, the probability of the CN formation decreases in the reactions induced by the heaviest projectile, at energies above the entrance barrier (Coulomb barrier + rotational energy). The decrease in the fusion cross-section is connected with an increase in the number of events going to quasifission. This last-mentioned process is a dominant one in reactions between massive nuclei and also in reactions induced by lighter ions at higher beam energies [6–9].

The basic difference between the fusion-fission and quasifission processes is that in the latter mechanism a dinuclear system formed at the capture stage cannot be transformed into a compound nucleus. Quasifission reactions are binary processes that exhibit some of the characteristics of fusion-fission events, such as full dissipation of the relative kinetic energy and a considerable transfer of mass between the two fragments. The amount and direction of the main nucleon flow depend on the landscape of the potential energy surface and shell structure.

Moreover, experimentally it is difficult to distinguish unambiguously the difference between fusion-fission and quasifission fragments which can be formed both in mass-symmetric and mass-asymmetric regions. Therefore, it is difficult to estimate the fusion cross-section from the measured data on the yield of fragments of symmetric masses assuming that the symmetric-mass fragments may be considered as products of the CN fusion-fission process.

Nevertheless, the dinuclear system concept (DNS) [10] allows us to estimate theoretically from the calculated capture cross-section a decrease in the number of events leading to complete fusion in competition with quasifission. The part of the capture cross-section, which produces the quasifission, increases drastically in reactions with massive nuclei [7,10] or with the nuclei of near-symmetric masses [10]. As a result, the difference between capture and fusion cross-sections increases sufficiently. In this case, an application of the well-known models [11,12]

[a] e-mail: giardina@nucleo.unime.it

to calculate the fusion cross-section is questionable though they were successfully used to calculate the fusion excitation functions in reactions with light and intermediate nuclei. The models [6–9], which were developed on the basis of the dinuclear system concept (DNS), can be used for all of the reactions mentioned above. For example, the results on the fusion excitation functions for ^{19}F + ^{107}Ag and ^{28}Si + ^{98}Mo reactions leading to ^{126}Ba [6] and the reactions leading to superheavy elements [7] were calculated by the same method of calculation. The different strength of the hindrance to fusion in different reactions is connected with the peculiarities of the driving potential, which is determined by the reaction Q_{gg}-value and nucleus-nucleus interaction potential [7–9]. So, there is not need to modify parameters of the code for numerical calculations at its application for reactions leading to ^{126}Ba or superheavy elements. Using the partial fusion cross-section $\sigma_\ell^{\rm fus}(E)$ obtained in the framework of a model [6–9] based on the DNS concept, we determine the competition between fission of the excited compound nucleus and evaporation residue formation along the CN de-excitation cascade using the advanced statistical model (ASM) [13–15].

In the present work, we consider two reactions with different entrance channel mass asymmetries ($\eta_A = (A_2 - A_1)/(A_1 + A_2)$) leading to the ^{220}Th* compound nucleus. We also compare the result of our calculations with the available experimental data [1–3].

The aim of this paper is to analyze the dependence of the evaporation residue formation on the partial fusion cross-section calculated at different beam energies comparing the theoretical results for the same excited compound nucleus ^{220}Th*. We found that the difference between the excitation functions of the evaporation residues formation is caused by:

i) the difference in partial fusion cross-section and angular-momentum distribution for the compound nucleus obtained as result of the two ^{16}O + ^{204}Pb and ^{96}Zr + ^{124}Sn reactions;

ii) the dependence of survival probability of the compound nucleus on its angular momentum.

The first cause is related to the height and size of the nucleus-nucleus potential well and the Q_{gg}-value of these reactions which determine the values of the intrinsic fusion barrier $B^*_{\rm fus}$ and the quasifission barrier $B_{\rm qf}$ [6–9]. The second cause is determined by the dependence of the fission probability $\Gamma_{\rm fis}/\Gamma_{\rm tot}$ of the ^{220}Th* compound nucleus on the $\sigma_\ell^{\rm fus}(E)$ distribution due to the dynamical effects in the entrance channel.

2 Method of calculation

According to the DNS concept, the evaporation residue production following a nuclear reaction is considered as a three-stage process. The first step is overcoming the Coulomb barrier by nuclei in the motion along the axis connecting nuclear centers at the in-coming stage of collision, and formation of a nuclear composite (the so-called molecular-like dinuclear system). This stage is called capture. The second stage is the transformation of the DNS into a more compact compound nucleus in competition with the quasifission process. At this stage, the system must overcome the intrinsic fusion barrier $B^*_{\rm fus}$ at the potential energy surface [7–9] during the evolution on the mass (charge) asymmetry axis. For light and intermediate nuclear systems or for heavy nuclear systems with larger mass asymmetries, this barrier is equal to zero and capture immediately leads to fusion. In these cases the fusion cross-section is calculated in the framework of well-known models [11,12]. It should be stressed that complete fusion is a transfer of all the nucleons of the projectile (or light nucleus) into the target.

At the third stage, the hot compound nucleus cools down by emission of neutrons and charged particles. There is a chance for the excited nucleus to undergo fission at each step of the de-excitation cascade. Therefore, the evaporation residue cross-section is determined by the partial fusion cross-sections and survival probabilities of the compound nucleus:

$$\sigma_{\rm er}(E) = \sum_{\ell=0}^{\ell_d} (2\ell+1)\sigma_\ell^{\rm fus}(E) W_{\rm sur}(E,\ell). \qquad (1)$$

The effects connected with the entrance channel are included in the partial fusion cross-section $\sigma_\ell^{\rm fus}(E)$, which is determined by the product of partial capture cross-sections and the related fusion factor ($P_{\rm CN}$) taking into account the competition between complete fusion and quasifission processes:

$$\sigma_\ell^{\rm fus}(E) = \sigma_\ell^{\rm capture}(E) P_{\rm CN}(E,\ell), \qquad (2)$$

where

$$\sigma_\ell^{\rm capture}(E) = \frac{\lambda^2}{4\pi} \mathcal{P}_\ell^{\rm capture}(E). \qquad (3)$$

Here λ is the de Broglie wavelength of the entrance channel; $\mathcal{P}_\ell^{\rm capture}(E)$ is the capture probability which depends on the collision dynamics and is determined by the number of partial waves ($\ell_{\rm d}$) leading to capture. We solve equations of motion for the relative distance R and the conjugate momentum [7–9]. In eq. (1), $W_{\rm sur}(E,\ell)$ is the survival probability against fission along the de-excitation cascade of CN.

Equation (1) is related to the first step of the de-excitation cascade of CN. The contribution of ER for the x-th step, characterized by the proton number Z_x and the neutron number N_x, reached after the emission from CN of particles νn+yp+$k\alpha$+$s\gamma$ (ν, y, k, s are numbers of neutrons, protons, α-particles and γ-quanta), is calculated by the expression

$$\sigma_{\rm er}^x(E) = \sum_{\ell=0}^{\ell_{\rm d}} (2\ell+1)\sigma_\ell^{x-1}(E) W_{\rm sur}^{x-1}(E,\ell), \qquad (4)$$

where $\sigma_\ell^{x-1}(E)$ is the partial formation cross-section of the excited intermediate nucleus of the $(x-1)$-th step and $W_{\rm sur}^{x-1}(E,\ell)$ is the survival probability of the $(x-1)$-th intermediate nucleus against fission along the de-excitation cascade of CN.

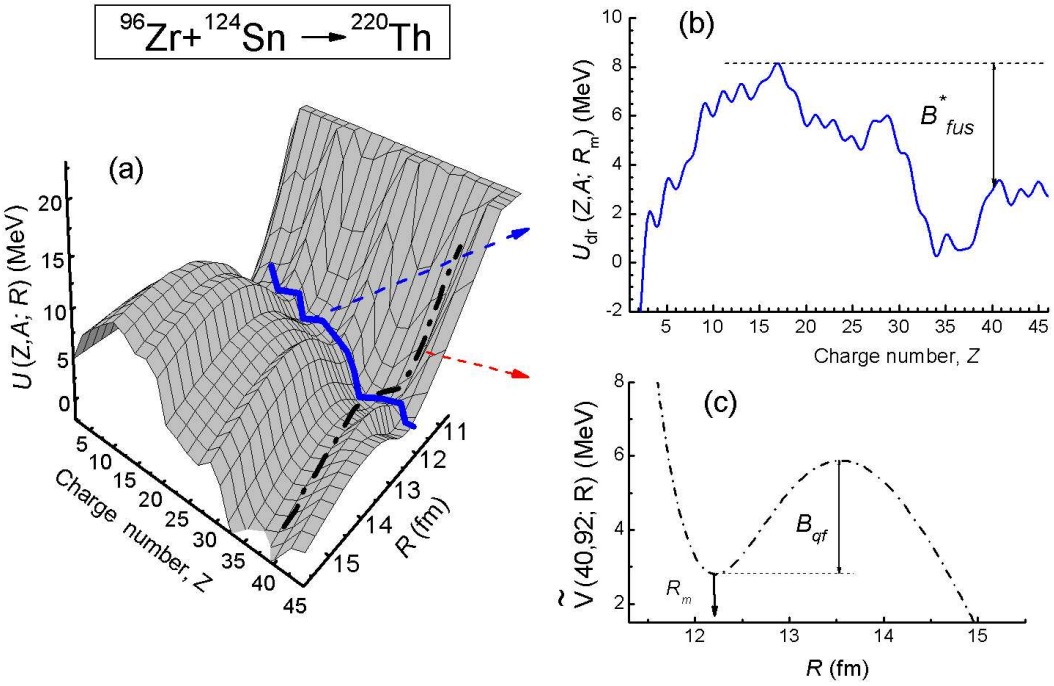

Fig. 1. The potential energy surface for a dinuclear system leading to the formation of the ^{220}Th* compound nucleus as a function of the relative distance R between centers of interacting nuclei and their charge numbers Z, panel (a); the driving potential, $U_{\rm dr}(Z, A, R_{\rm m})$, which is a curve connecting minimums of the potential energy surface as a function of Z, panel (b); the nucleus-nucleus interaction potential $U(R)$ shifted on Q_{gg}-value for the ^{96}Zr + ^{124}Sn reaction, panel (c).

A more detailed description of the method is given in refs. [6–9]

The intrinsic fusion barrier $B^*_{\rm fus}$ is connected with mass (charge) asymmetry degrees of freedom of the dinuclear system and is determined from the potential energy surface (fig. 1). The potential energy surface is built as a function of the charge number $Z = Z_1$ of one of the fragments forming DNS ($Z_2 = Z_{\rm CN} - Z$, $Z_{\rm CN}$ is the charge of compound nucleus) and the relative distance between their centers

$$\begin{aligned} U(Z, A; R, L) &= U(Z, A\ell, \beta_1, \alpha_1; \beta_2, \alpha_2) \\ &= B_1 + B_2 + V(Z, A, L, \beta_1, \alpha_1; \beta_2, \alpha_2; R) \\ &\quad -(B_{\rm CN} + V_{\rm CN}(L)). \end{aligned} \tag{5}$$

Here, B_1, B_2 and $B_{\rm CN}$ are the binding energies of the nuclei in DNS and of the CN, respectively, which were obtained from [16,17]; β_i are the fragment deformation parameters taken from the tables in [17–19] and α_i are the orientations relative to the beam direction (see App. A of ref. [8]); $V_{\rm CN}(L)$ is the rotational energy of the compound nucleus. The distribution of neutrons between two fragments for the given proton numbers Z and Z_2 (or ratios A/Z and A_2/Z_2 for both fragments, where $A = A_1$, $A_2 = A_{\rm CN} - A$, and $A_{\rm CN}$ is the mass of the compound nucleus) was determined by minimizing the potential $U(Z, A; R)$ as a function of A for each Z.

The potential energy surface $U(Z, A; R, L = 0)$, calculated in this way for the ^{220}Th CN, is presented in fig. 1a. $B^*_{\rm fus}$ is determined by the difference between the maximum value of the driving potential $U(Z, A, R_{\rm m})$ and its value at the point corresponding to the initial charge asymmetry of the considered reaction (see fig. 1b). The driving potential $U(Z, A, R_{\rm m})$ is extracted from the potential energy surface $U(Z, A; R, L)$ (5) as a function of the charge number Z of its minimum values corresponding to the minima of nucleus-nucleus potential $V(R)$ [6–9] (see the solid curve at the bottom of the potential valley in fig. 1a) for the given charge asymmetry. The position of this minimum on the relative distance between nuclei is $R = R_{\rm m}$ (fig. 1c). In fig. 1c, the curve of nucleus-nucleus potential is presented for the ^{96}Zr + ^{124}Sn reaction and its values are shifted on the Q_{gg}-value of this reaction: $\tilde{V}(40, R) = U(40, 92; R, L = 0) + B_1 + B_2 - B_{\rm CN}$. If the excitation energy of the dinuclear system ($E^*_{\rm DNS} = E_{\rm c.m.} - V(R_{\rm m}, L)$) is not enough for overcoming $B^*_{\rm fus}$, the dinuclear system decays into two fragments and undergoes quasifission after nucleon exchange between its components. The quasifission occurs due to motion along the relative internuclear

distance R and depends on the nucleus-nucleus interaction potential $V(R)$. At capture, the DNS is in the potential well. Thus, in order that the quasifission occurs, it is necessary to overcome the barrier $B_{\rm qf}$ which is equal to the depth of the well of $V(R)$ (fig. 1c). If the DNS excitation energy is not enough for overcoming $B_{\rm qf}$, it fluctuates on the charge asymmetry axis moving to a more symmetric configuration. A DNS can decay more easily into two fragments due to a decrease in $B_{\rm qf}$ increasing the charge symmetry. The driving potential containing these characteristics under discussion is significant in considering the fusion process as a motion of the system along the mass (charge) asymmetry degree of freedom. The dependence of $B^*_{\rm fus}$ on the orbital angular momentum affects the partial cross-sections of fusion: $B^*_{\rm fus}$ increases and $B_{\rm qf}$ decreases by increasing of L. As a result the fusion factor $P_{\rm CN}$ decreases by increase of orbital angular momentum. For the more symmetric reactions this effect appears more strongly [8]. The fusion probability $P_{\rm CN}(E,\ell)$ (or the fusion factor, in eq. (2)) in competition with the quasifission process can be calculated using the level density and potential energy surface. The probability of realizing the complete fusion process is related to the ratio of the level densities, depending on the intrinsic fusion or quasifission barriers, by the expression [7–9]:

$$P_{\rm CN} = \frac{\rho(E^*_{\rm DNS} - B^*_{\rm fus})}{\rho(E^*_{\rm DNS} - B^*_{\rm fus}) + \rho(E^*_{\rm DNS} - B_{\rm qf})}, \qquad (6)$$

where $\rho(E^*_{\rm DNS} - B^*_{\rm K})$ is the DNS level density which is calculated on the quasifission and intrinsic fusion barriers ($B_{\rm K} = B_{\rm qf}, B^*_{\rm fus}$). Taking into account the dependence of $B^*_{\rm fus}$ and $B_{\rm qf}$ on the angular momentum L, the factor $P_{\rm CN}$, being a function of these barriers and determining the competition between complete fusion and quasifission, decreases with increasing L at given values of the beam energy.

Due to dependence of the nucleus-nucleus potential on orientations of the axial symmetry of the deformed nuclei, the excitation function of the capture and fusion are sensitive to these orientations. The final results of the capture and complete fusion are obtained by averaging the contributions of different mutual orientations of the symmetry axis of the reacting nuclei.

The survival probability $W_{\rm sur}(E,\ell)$ is related to the partial fusion cross-section which affects the fission barrier and the $\Gamma_{\rm n}/\Gamma_{\rm tot}$ ratio too; the latter determines the evaporation residue production along the CN de-excitation cascade. At calculating of $W_{\rm sur}(E,\ell)$ in the framework of the advanced statistical model [13–15] $\sigma^{\rm fus}_\ell(E)$ is used as input data.

For the fission barriers, we use predictions of the rotating droplet model (angular-momentum–dependent) as parameterized by Sierk [20] and the dependences of the shell corrections [14] on the angular momentum and temperature. This is expressed by the formula for the actual fission barrier used in calculations:

$$B_{\rm fis}(L,T) = c\ B^{\rm m}_{\rm fis}(L) - h(T)\ q(L)\ \delta W, \qquad (7)$$

which includes dependence of the compound nucleus on the temperature and the orbital angular momentum by the following relations:

$$h(T) = \begin{cases} 1\,, & T \le 1.65\,{\rm MeV}\,, \\ k\exp\left(-mT\right), & T > 1.65\,{\rm MeV}\,, \end{cases}$$

$$q(L) = \{1 + \exp[(L - L_{1/2})/\Delta L]\}^{-1}, \qquad (8)$$

where $B^{\rm m}_{\rm fis}(L)$ is the parameterized macroscopic fission barrier [20] depending on the angular momentum L, $\delta W = \delta W_{\rm sad} - \delta W_{\rm gs} \simeq -\delta W_{\rm gs}$ is the microscopic (shell) correction to the fission barrier taken from the tables [17]; the constants for the macroscopic fission barrier scaling, temperature and angular-momentum dependencies of the microscopic correction are chosen as follows: $c = 1.0$, $k = 5.809$, $m = 1.066$ MeV^{-1}, $L_{1/2} = 24\hbar$ for the nuclei with $Z \simeq 80$–100 (or $L_{1/2} = 20\hbar$ for the nuclei with $Z > 100$), and $\Delta L = 3\hbar$. This procedure allows the shell corrections to become dynamical quantities too. In the present ASM calculations, the target-projectile fusion cross-section is determined directly by eq. (2) which gives the fusion spin distribution.

The code is able to calculate the Γ_ν ($\nu = n, p, \alpha \ldots$) and $\Gamma_{\rm fis}$ widths (see ref. [13]) at each step of the de-excitation cascade of the compound nucleus. $\Gamma_{\rm tot}$ is equal to $\Gamma_{\rm fis} + \sum \Gamma_\nu$.

In respect of the previous calculations [13], where a free parameter was used to describe the fallout of the fusion cross-section in the vicinity of $\ell_{\rm fus}$, we do not use such a free parameter because the study of the entrance channel dynamics gives the fusion spin distribution.

3 Results and discussion

In this section, we present the results obtained for the ^{220}Th* compound nucleus formed in the ^{16}O + ^{204}Pb and ^{96}Zr + ^{124}Sn reactions with different mass asymmetries in the entrance channel. The dependencies of the partial capture cross-section $\sigma^{\rm cap}_\ell(E)$, the partial fusion cross-section $\sigma^{\rm fus}_\ell(E)$, the fission probability $\Gamma_{\rm fis}/\Gamma_{\rm tot}$ of the excited intermediate nuclei along the de-excitation cascade of the compound nucleus, and the evaporation residue production on the entrance channel effects are discussed.

3.1 The capture and fusion cross-sections

Using relations (2) and (3), we calculate the partial capture $\sigma^{\rm cap}_\ell(E)$ and fusion $\sigma^{\rm fus}_\ell(E)$ cross-sections for the ^{16}O + ^{204}Pb and ^{96}Zr + ^{124}Sn reactions. The main parameters which characterize the entrance channel for these reactions leading to the ^{220}Th* compound nucleus are presented in table 1.

In fig. 2, we present and compare the calculated capture and fusion cross-sections for the above-mentioned reactions. The figure shows the difference between the capture cross-sections (panel a) for the two reactions having different mass asymmetries in the entrance channel.

Table 1. Charge asymmetry (η_Z), intrinsic fusion ($B^*_{\rm fus}$) and quasifission ($B_{\rm qf}$) barriers, and fusion factor ($P_{\rm CN}$) for the two reactions leading to the ^{220}Th* CN, at $E^* = 55$ MeV.

Reactions	η_Z	$B^*_{\rm fus}$ (MeV)	$B_{\rm qf}$ (MeV)	$P_{\rm CN}$
^{16}O + ^{204}Pb	0.822	0	17.7	0.99
^{96}Zr + ^{124}Sn	0.111	5.3	5.4	0.13

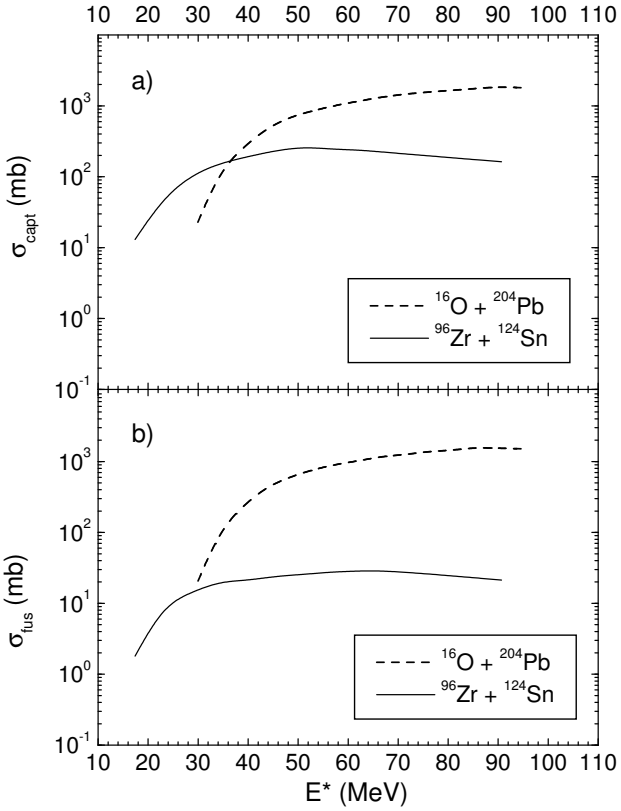

Fig. 2. Comparison of the capture (panel a) and fusion (panel b) cross-sections for the ^{16}O + ^{204}Pb and ^{96}Zr + ^{124}Sn reactions leading to ^{220}Th*.

The maximum value of the capture excitation function for the ^{96}Zr + ^{124}Sn reaction is lower than that for the ^{16}O + ^{204}Pb reaction, due to smallness of the potential well for the first reaction. The number of partial waves ℓ is determined by the size of the well in the nucleus-nucleus potential. In our calculations, the depth of the potential well is accepted as a quasifission barrier $B_{\rm qf}$. This barrier is sufficiently higher for the ^{16}O + ^{204}Pb reaction ($B_{\rm qf} = 17.7$ MeV) than in the case of the ^{96}Zr + ^{124}Sn one ($B_{\rm qf} = 5.4$ MeV, see table 1). The high quasifission barrier $B_{\rm qf}$ promotes the formation of the compound nucleus having a higher angular momentum at large beam energies. As one can see, there are different excitation energy ranges for the compound nucleus formed as a result of these two reactions. The fusion excitation function for the ^{96}Zr + ^{124}Sn reaction (solid line in fig. 2, panel b) is much lower than that for the ^{16}O + ^{204}Pb reaction (dashed line in the same panel b), because the fusion factor $P_{\rm CN}$ (6) for the ^{16}O + ^{204}Pb reaction is greater than that for the ^{96}Zr + ^{124}Sn reaction (see table 1). The values of the intrinsic fusion and quasifission barriers strongly affect the factor $P_{\rm CN}$: a small value of $B^*_{\rm fus}$ and a great value of $B_{\rm qf}$ are favorable for the complete fusion. The structure and shape of $\sigma^{\rm fus}_\ell(E)$ for the same excited compound nucleus formed in different reactions are sensitive to dynamical effects in the entrance channel. Therefore, comparison of results obtained for different reactions leading to the same compound nucleus clarifies the reaction mechanism. Theoretical analysis shows that the choice of the beam energy for the production of the compound nucleus with the same excitation energy in different reactions does not allow one to obtain the same values for the partial fusion cross-sections. In fig. 3, these dynamical effects are shown as a dependence of the partial capture $\sigma^{\rm cap}_\ell(E)$ and fusion $\sigma^{\rm fus}_\ell(E)$ cross-sections calculated for the two different reactions on the excitation energy and angular momentum. Comparison of the two panels shows that the shape, yield, volume and structure of the $\sigma^{\rm fus}_\ell(E)$ are quite close in shape, volume and structure of $\sigma^{\rm cap}_\ell(E)$ for the ^{16}O + ^{204}Pb reaction, whereas the partial $\sigma^{\rm fus}_\ell(E)$ cross-section greatly differs in shape, yield, volume and structure of the $\sigma^{\rm cap}_\ell(E)$ cross-section for the ^{96}Zr + ^{124}Sn reaction.

This result is connected with different intrinsic and quasifission barriers determining fusion-quasifission competition for the two reactions under discussion. In addition, from fig. 4a (for the ^{16}O + ^{204}Pb reaction) one can see that the contribution of the quasifission process is not so much in the more mass-asymmetric reaction in comparison with the massive contribution of the quasifission in the more symmetric reaction (see fig. 4b, for the ^{96}Zr + ^{124}Sn reaction).

In any case, the effect of the quasifission process appears at the low angular-momentum values (6–8$\hbar$) for both reactions and the process becomes more intensive at large values of L (see fig. 4a, b). Of course, the number of events going to quasifission increases for the reaction induced by the heavier projectile. Moreover, as one can see in the left bottom panel of fig. 3, the $\sigma^{\rm fus}_\ell(E)$ has a larger volume in the ^{16}O + ^{204}Pb reaction as compared with the ^{96}Zr + ^{124}Sn reaction (right bottom panel). Generally, the partial fusion cross-section for the ^{16}O+ ^{204}Pb reaction extends to higher angular-momentum values due to high quasifission barrier (see table 1). The partial fusion cross-section for the ^{96}Zr + ^{124}Sn reaction extends to higher angular-momentum values in comparison with those in the ^{16}O + ^{204}Pb reaction at the excitation energies E^* lower than about 45 MeV. There is no capture for great L values because the fusion barrier in the entrance channel is higher than the beam energies corresponding to the excitation energy range $E^* < 45$ MeV for the reaction induced by ^{16}O.

Therefore, different entrance channels leading to the same excited compound nucleus do not generally produce the same evaporation residue cross-section, due to the dependence of the survival probability (related to the

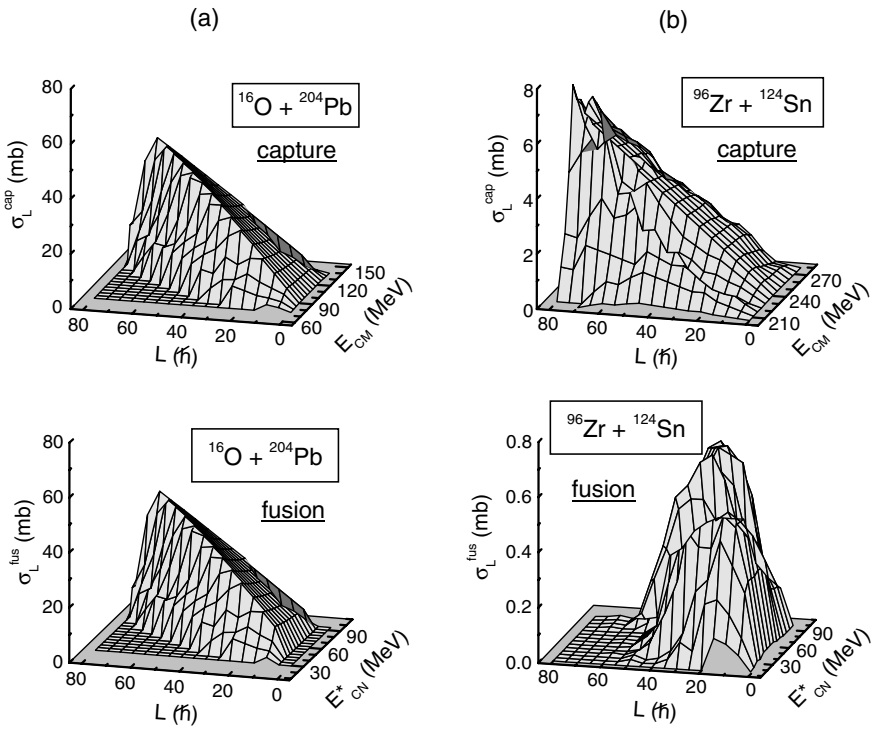

Fig. 3. Partial capture ($\sigma_\ell^{\rm cap}(E)$) and fusion ($\sigma_\ell^{\rm fus}(E)$) cross-sections for the $^{16}O + ^{204}Pb$ and $^{96}Zr + ^{124}Sn$ reactions leading to $^{220}Th^*$, at various beam energies that give the same excitation energy range of CN.

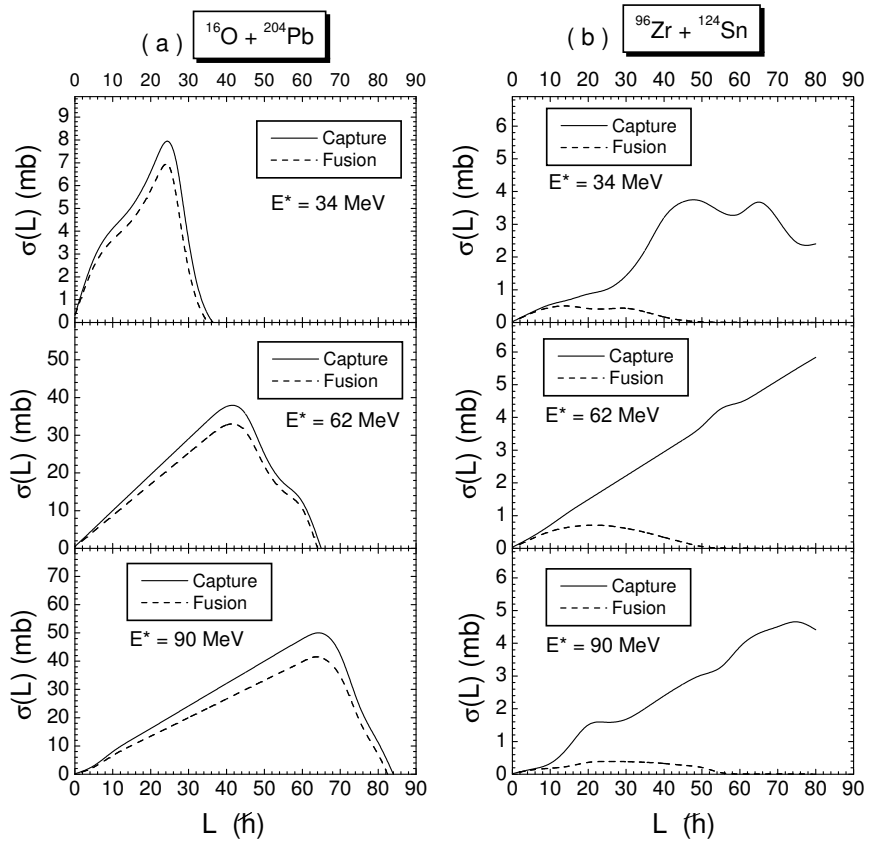

Fig. 4. Comparison between the partial capture $\sigma_\ell^{\rm cap}(E)$ (full line) and fusion $\sigma_\ell^{\rm fus}(E)$ (dashed line) cross-sections for the $^{16}O + ^{204}Pb$ and $^{96}Zr + ^{124}Sn$ reactions leading to the $^{220}Th^*$ CN, formed at the excitation energy E^* of 34, 62 and 90 MeV. The difference between the two lines is the quasifission contribution.

$\Gamma_\nu/\Gamma_{\rm tot}$ values at all steps of the de-excitation cascade) on the angular-momentum distribution of CN. Consequently, the fission probability of the ^{220}Th* compound nucleus formed in these two reactions is a function of the $\sigma_\ell^{\rm fus}(E)$ distribution and depends on the dynamical effect in the entrance channel.

3.2 Dependence of the nucleus fission probability on the entrance channel

In fig. 5 we present the fission probability $\Gamma_{\rm fis}/\Gamma_{\rm tot}$ against E^* for the ^{220}Th* CN obtained as a result of the ^{16}O + ^{204}Pb and ^{96}Zr + ^{124}Sn reactions. There are two main effects which will be analyzed:

i) a big difference between fission probability values of the excited ^{220}Th* formed in these reactions at excitation energies $E^* < 45$ MeV;

ii) a decrease in fission probability values for both reactions at about $E^* > 45$ MeV.

At lower excitation energies ($E^* < 45$ MeV) the fission probability of the CN for the ^{96}Zr + ^{124}Sn reaction is about 1.3–4.5 times higher than that for the ^{16}O + ^{204}Pb reaction. The increase in the difference between the $\Gamma_{\rm fis}/\Gamma_{\rm tot}$ values for the reactions under discussion with decreasing the excitation energy is due to different sets of the orbital angular momentum which contribute to $\sigma_\ell^{\rm fus}(E)$ for the ^{16}O + ^{204}Pb and ^{96}Zr + ^{124}Sn reactions in the energy range under discussion (see fig. 3, bottom panels). Due to the large moment of inertia of the dinuclear system formed in the ^{96}Zr + ^{124}Sn reaction, an increase in the entrance barrier value (Coulomb barrier + rotational energy) is not so much at the high angular momentum $L = 30\hbar$ which decreases appreciably the fission barrier by $q(L)$ in eq. (7). Instead, the small moment of inertia of the dinuclear system formed in the ^{16}O + ^{204}Pb reaction does not allow contributions of the high angular momentum to capture and fusion at energies close the Coulomb barrier (top panel of fig. 3a). Dependence of shell corrections on the rotational energy of the compound nucleus presented by the factor $q(L)$ in eq. (8) is strong around $L = L_{1/2} = 24\hbar$. It is well known that both of the liquid-drop [20] and shell correction (7) components of the fission barrier decreases by increasing of L. For example, at $L = 24\hbar$ the shell corrections causing a decrease in the fission barrier by half, and at about $L = 40\hbar$ these corrections are washed-out. The high fission probability of the compound nucleus formed in the ^{96}Zr + ^{124}Sn reaction at $E^* < 45$ MeV is explained by the strong decrease in fission barrier value at the high angular momentum which contributes to $\sigma_\ell^{\rm fus}(E)$ (top panel of fig. 3b). At lower excitation energies ($E^* < 45$ MeV), the fission probability of nuclei at the first, second and third steps of the cascade is higher for the de-excitation of the CN formed in the ^{96}Zr + ^{124}Sn reaction (characterized by a larger set of angular-momentum values which reduces the fission barrier) as compared with the fission probability of the corresponding nuclei in the cascade of the CN produced in the more asymmetric ^{16}O + ^{204}Pb reaction. This is the reason of the different behaviour of the fission probability $\Gamma_{\rm fis}/\Gamma_{\rm tot}$ in mass-asymmetric and mass-symmetric reactions.

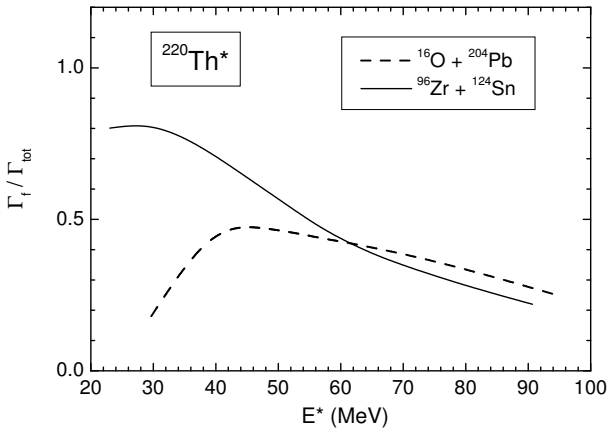

Fig. 5. Comparison of the fission probability ($\Gamma_{\rm fis}/\Gamma_{\rm tot}$) values *versus* the excitation energy E^* of the ^{220}Th* compound nucleus obtained by the ^{16}O + ^{204}Pb and ^{96}Zr + ^{124}Sn reactions.

The slow decrease in fission probability of CN at higher excitation energies ($E^* > 45$ MeV) for both these reactions is explained mainly by an increase in neutron emission which cools the excited compound nucleus. We calculated the $\Gamma_{\rm fis}/\Gamma_{\rm tot}$ ratio at each step along the de-excitation cascade of the compound nucleus as well as the excitation function of the evaporation residues. Of course, the production of ER is strongly related to the energy dependence of the partial fusion cross-section $\sigma_\ell^{\rm fus}(E)$ and $\Gamma_{\rm n}/\Gamma_{\rm tot}$ values at all steps of the de-excitation cascade of the ^{220}Th* CN.

Figure 5 also shows that in the $E^* > 65$ MeV energy range, the $\Gamma_{\rm fis}/\Gamma_{\rm tot}$ values of the CN for the ^{16}O + ^{204}Pb reaction are about 1.1–1.2 times greater than those for the ^{96}Zr + ^{124}Sn reaction, because the angular-momentum range giving contribution to $\sigma_\ell^{\rm fus}(E)$ for the ^{16}O + ^{204}Pb reaction is wider than that of the ^{96}Zr + ^{124}Sn reaction (see middle panels of fig. 4a and b).

In fig. 6 we present the calculated fission probability $\Gamma_{\rm fis}/\Gamma_{\rm tot}$ of the excited intermediate nuclei along the de-excitation cascade of the ^{220}Th* compound nucleus (after neutron emissions) produced in the ^{16}O + ^{204}Pb and ^{96}Zr + ^{124}Sn reactions.

This figure shows the changing of the fission probability of each intermediate excited nucleus reached by the two reactions along the de-excitation cascade of the compound nucleus after x neutron emission. Panels a), b), c) and d) show a noticeable difference in the fission probability of each excited nucleus reached by the two reactions in the first steps of the cascade; instead the panels e), f), g) and h) show that the fission probability of remaining excited nuclei at the last steps of the cascade are comparable for the two reactions.

This behaviour is due to the fact that at relatively lower excitation energies of CN (for example at $E^*_{\rm x} <$ 50 MeV), the fission probability of the intermediate nuclei formed along the de-excitation of CN (that is obtained

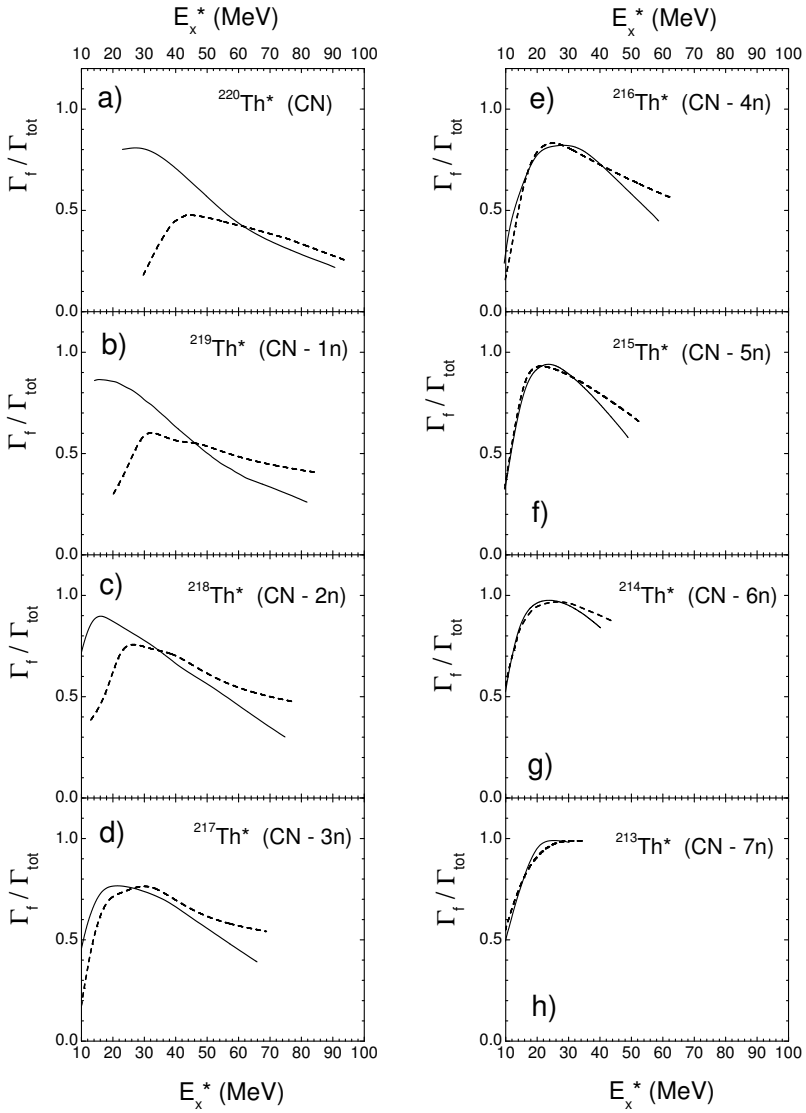

Fig. 6. Comparison of the $\Gamma_{\rm fis}/\Gamma_{\rm tot}$ fission probability values for each step of the de-excitation cascade after neutron emission only of the ^{220}Th* compound nucleus reached by the ^{16}O + ^{204}Pb and ^{96}Zr + ^{124}Sn reactions. Panel a) is related to the ^{220}Th (CN) fission probability; panel b) is related to the fission probability of the excited ^{219}Th* nucleus (CN-1 neutron); ... panel h) is related to the fission probability of the excited ^{213}Th* (CN-7 neutrons). On the abscissa axis are reported the $E^{*}_{\rm x}$ excitation energy values of nuclei formed along the de-excitation cascade of CN (dashed lines are related to ^{16}O + ^{204}Pb reaction; solid lines are related to ^{96}Zr + ^{124}Sn reaction).

by the two reactions) at $E^{*}_{\rm x} < 40$, 30, 20 MeV after 1, 2 and 3 neutron emission, respectively, see panels b), c), d)) is strongly related to the different angular-momentum sets populated in the reactions under discussion. In this last-mentioned low energy range of E^{*}, the values of L are wider for the nuclei coming from the chain of the ^{96}Zr + ^{124}Sn reaction and its fission probabilities (solid lines in fig. 6) are higher than the ones of the corresponding nuclei coming from the chain of the ^{16}O + ^{204}Pb reaction (dashed lines in fig. 6). At each step of the cascade from CN to CN-3n, the differences between the fission probabilities (full and dashed lines) of each excited intermediate nucleus formed by the two considered reactions are reduced because each neutron emission cools the nuclear system also reducing the difference between the angular-momentum sets related to the dynamics of the entrance channel for the two reactions.

At relatively higher excitation energies E^{*} of CN (for example at about 70–80 MeV, allowing for a more large multiple neutron emission), the first steps of the cascade after 1-3 neutron emission lead to intermediate nuclei with excitation energies between 70–40 MeV. The appreciable difference in the fission probability of each intermediate nucleus (see panels b), c), d) of the same figure) formed by the two considered reactions (full and dashed lines) is related to the different angular-momentum ranges that contribute to the formation cross-sections of intermediate nuclei along the cascade. But in this considered excitation

energy range, the angular-momentum set is higher for the $^{16}O + {}^{204}Pb$ reaction than for the $^{96}Zr + {}^{124}Sn$ reaction, starting from the compound nucleus formation (see middle and bottom panels of fig. 4). Therefore, the fission probability (dashed line) of each excited intermediate nucleus formed by the $^{16}O + {}^{204}Pb$ reaction is higher than the fission probability (full line) of the corresponding intermediate nucleus formed by the $^{96}Zr + {}^{124}Sn$ reaction. Of course, after 4–7 neutron emission the excitation energy of the intermediate nuclei is reduced to about 40–10 MeV, and the fission probabilities (dashed and full lines) of the last remaining intermediate nuclei ($^{216}Th^*$–$^{213}Th^*$) of the cascade are comparable for each nucleus formed by the two mentioned reactions. Also in such a case, the result on the fission probability is strongly related to the cooling of the nuclear system and the comparable angular-momentum sets that contribute to the formation of each intermediate nucleus by the two reactions under consideration.

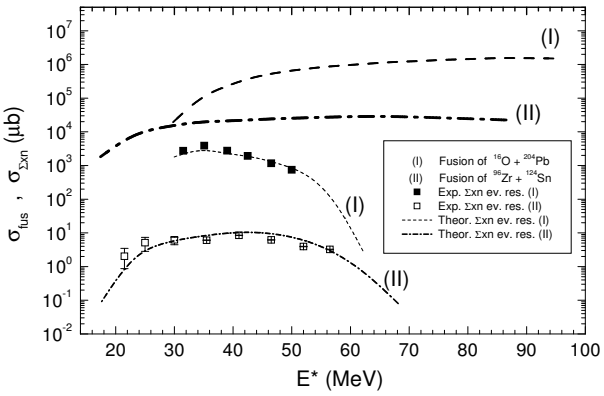

Fig. 7. Comparison of evaporation residues for the $^{16}O + {}^{204}Pb$ and $^{96}Zr + {}^{124}Sn$ reactions leading to the $^{220}Th^*$ CN. The experimental data of the evaporation residues are taken from refs. [1,3].

3.3 Evaporation residue cross-sections

In fig. 7, the total evaporation residues (immediately after the neutron emission along the de-excitation cascade of the compound nucleus) calculated by us are compared with the experimental data [1–3] for the above-mentioned reactions leading to $^{220}Th^*$. The difference between the evaporation residue cross-sections for the two reactions at each value of the excitation energy E^* is explained by the difference in the fusion cross-sections caused by the peculiarities of the entrance channel and different fission probability of the compound nucleus produced in the two reactions. In fact, in the energy region $E^* > 60$ MeV of $^{220}Th^*$, the ratio between the fusion and the evaporation residue cross-sections of the $^{16}O + {}^{204}Pb$ reaction is about 10^5, whereas the corresponding ratio for the $^{96}Zr + {}^{124}Sn$ reaction is about 10^4. It is connected with a higher fission probability of CN for the $^{16}O + {}^{204}Pb$ reaction (see fig. 5) at the high angular momenta ($L_{max} \simeq 80\hbar$, bottom left panel of fig. 3) which causes a strong decrease of the CN fission barrier, whereas for the $^{96}Zr + {}^{124}Sn$ reaction L_{max} of CN is less than $60\hbar$ in the same excitation energy range.

On the contrary, in the energy range $E^* < 45$ MeV of $^{220}Th^*$, the ratio between the fusion and the evaporation residue cross-sections of the $^{16}O + {}^{204}Pb$ reaction is about 10^2, whereas the corresponding ratio for the $^{96}Zr + {}^{124}Sn$ reaction is about 10^3. This circumstance is caused by a higher fission probability of CN and other excited intermediate nuclei formed along the de-excitation cascade of the compound nucleus produced in the $^{96}Zr + {}^{124}Sn$ reaction (characterized by a large set of angular momenta), as compared (see fig. 5) with the corresponding values for the cascade of CN produced in the $^{16}O + {}^{204}Pb$ reaction (characterized by a smaller set of angular momenta) at $E^* < 45$ MeV.

As a result of an overall inspection of fig. 7, one can see that at about $E^* = 30$ MeV, when the fusion cross-sections of the two reactions reach the same value, the residue cross-sections differ greatly; on the contrary, at about $E^* = 64$ MeV the calculated residue cross-sections reach the same values, whereas the fusion cross-sections of the two reactions are characterized by a relevant and increasing difference of values. It is mainly the result of a different trend in fission probability of the compound nucleus and the other two-three subsequent excited intermediate nuclei after 1, 2 and 3 neutron emission. Therefore, the yield of ER, at lower and higher excitation energies E^* of CN, is mainly affected by different trends of fission probability of the excited nuclei along the first three steps of the de-excitation cascade of CN (see the related full and dashed lines of fig. 6). We should stress that so far no author has stated that some difference in the ER production is due also to the different behaviour of CN fission probability at the same E^*. On the contrary, it is believed that mainly the last step of the de-excitation cascade determines the yield of ER, whereas we should like to affirm here that the formation at last step is strongly affected by the first steps of the de-excitation cascade of CN. Therefore, usually it is affirmed that low values of L (up to about $15\hbar$) contribute to the ER and then different reactions in the entrance channel forming the same CN with the same E^* have to produce about the same ER. When this result is not confirmed in experiments with reactions of the different mass asymmetry in the entrance channel, some authors (see, for example, refs. [1,2]) affirm that this is due to partial inhibition of the fusion process caused by competition with quasifission. This is true but partially. In fact, if we normalize the ER production to the fusion cross-section (σ_{er}/σ_{fus}) we find that there still remain large differences between the reduced values of the ER production for the two reactions. For example, in fig. 7, at $E^* = 34$ MeV, the σ_{er}/σ_{fus} is about $3.5 \cdot 10^{-4}$ for the $^{96}Zr + {}^{124}Sn$ reactions, whereas it is about $5 \cdot 10^{-2}$ for the $^{16}O + {}^{204}Pb$ reaction. This large difference between the reduced values of ER is due to the relevant different fission probabilities of the same CN produced in the above mentioned reactions (see the first steps of fig. 6 at $E^* = 34$–14 MeV) and the same excited intermediate nuclei along the cascade.

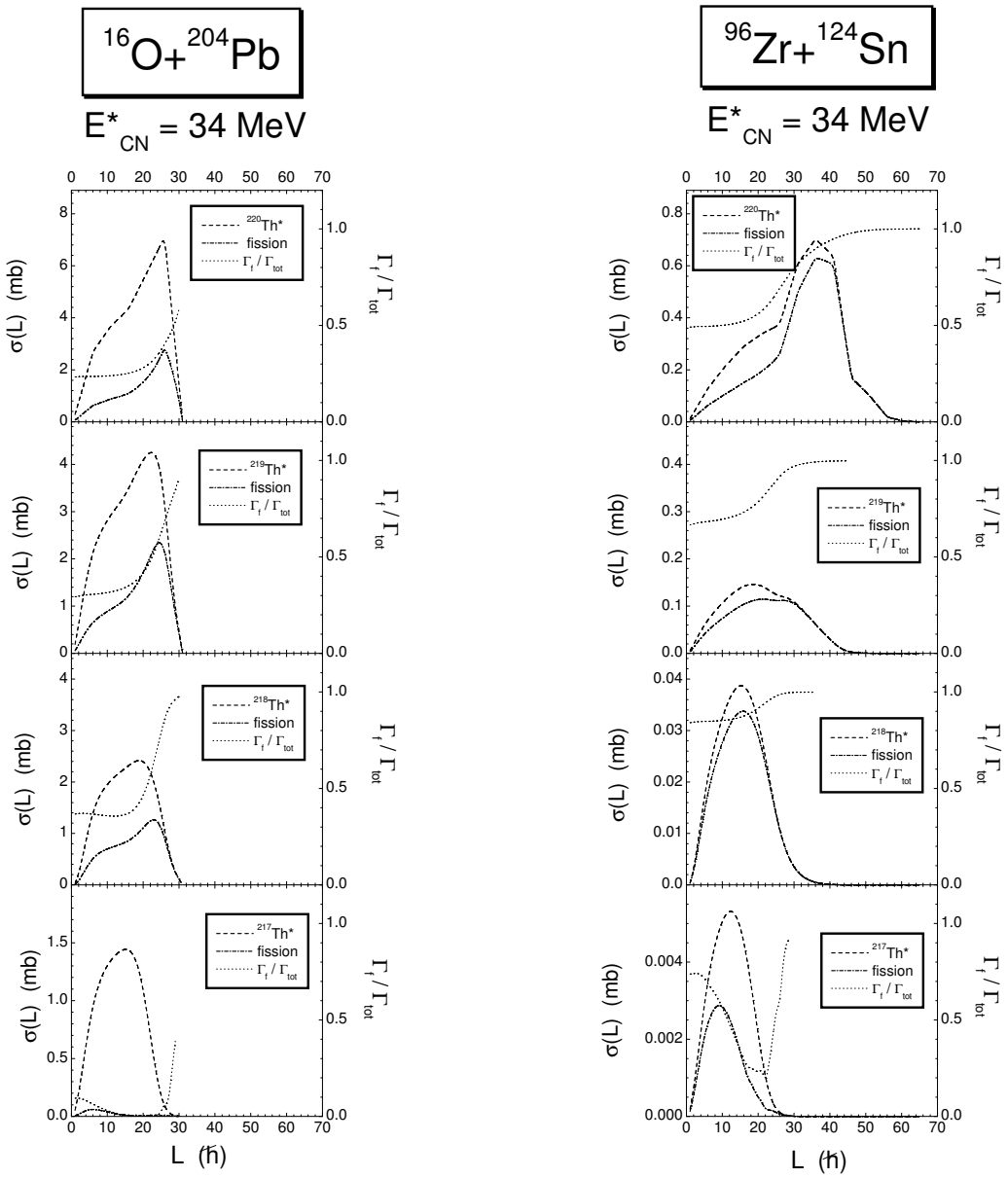

Fig. 8. Comparison of the formation (dashed line) and fission (dash-dotted line) cross-sections for the excited nuclei formed along the de-excitation cascade of the ^{220}Th* compound nucleus produced in the ^{16}O + ^{204}Pb and ^{96}Zr + ^{124}Sn reactions at the CN excitation energy E^* of 34 MeV against L. The dotted line (on the right-hand ordinate scale) shows the change in the fission probability $\Gamma_{\rm fis}/\Gamma_{\rm tot}$ of each nucleus *versus* the orbital angular momentum L.

Figure 8 shows the partial cross-sections of the formation of CN and the excited intermediate nuclei in the ^{16}O + ^{204}Pb and ^{96}Zr + ^{124}Sn reactions at $E^* = 34$ MeV (dashed line, on the left-hand ordinate scale), and their fission cross-sections along the various steps of the de-excitation cascade (dash-dotted line, on the left-hand scale). The same figure also shows the fission probability distribution $\Gamma_{\rm fis}/\Gamma_{\rm tot}(L)$ (dotted line, on the right-hand ordinate scale) for each L. Comparing step-by-step results of the two reactions, one can see a different rate of the fission contribution with respect to the contribution of the excited intermediate nucleus formation. It is connected with a different fission probability distribution for each corresponding step of the cascades of CN produced in the two reactions, and with a change in the fission probability distribution of nuclei along various steps of the same cascade of CN. Comparing the cascades of the two reactions, one can see that the fission probability distribution values are higher for the excited nuclei produced in the more symmetric reaction. Within each de-excitation cascade, the fission probability increases in the subsequent steps at lower L values. Moreover, the last step of the neutron emission cascade also represents the orbital angular-momentum distribution of the evaporation

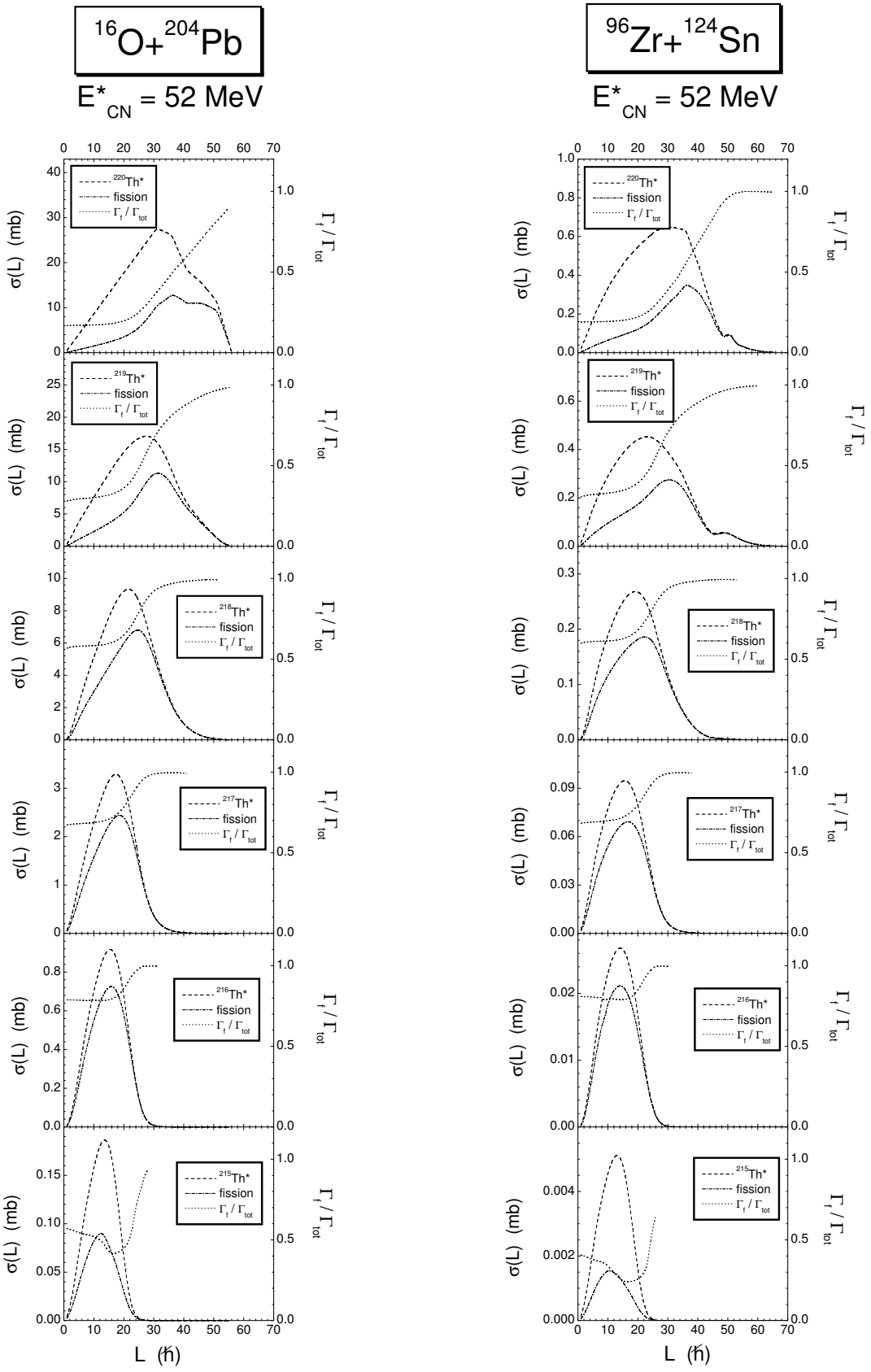

Fig. 9. As fig. 8, but for $E^* = 52$ MeV.

residue nucleus formed after the γ-cascade of the ^{217}Th*. This figure also shows that the evaporation residues are contributed by values of the orbital angular momentum up to about 32–36$\hbar$ units for the two ^{16}O + ^{204}Pb and ^{96}Zr + ^{124}Sn reactions, respectively.

Figure 9 shows the same as in fig. 8, but for the case of a higher excitation energy ($E^* = 52$ MeV) of the ^{220}Th* compound nucleus. At high value of the excitation energy E^*, the fission probability distribution $\Gamma_{\rm fis}/\Gamma_{\rm tot}(L)$ is comparable with the corresponding steps of the two reactions, and the contribution of $\Gamma_{\rm fis}/\Gamma_{\rm tot}(L)$ at lower L values increases for the subsequent steps of the same cascade. The rate of the fission yield (dash-dotted line), in comparison with the excited intermediate nucleus formation (dashed line), is comparable for the two reactions too; moreover, the evaporation residues are contributed by values of the orbital angular momentum up to about 28$\hbar$ for the two reactions. In this figure, the last panel gives information on the orbital angular-momentum distribution of the evaporation residue nucleus produced after the γ-cascade of ^{215}Th*.

4 Conclusions

We analyzed the cross-sections for the whole chain of the fusion-fission process for the two reactions (^{16}O + ^{204}Pb and ^{96}Zr + ^{124}Sn) having different mass asymmetries in the entrance channel: from the capture and fusion cross-sections up to the evaporation residue cross-section along the de-excitation cascade of CN through intermediate nuclei. Within the framework of the dinuclear system concept, we calculated the partial capture cross-section $\sigma_\ell^{\rm cap}(E)$ and the quasifission-fusion competition $P_{\rm CN}$ characterized by the intrinsic fusion barrier $B^*_{\rm fus}$ and the quasifission barrier $B_{\rm qf}$, taking into account dynamical effects of the entrance channel. We analyzed how various values of the orbital angular momentum leading to capture and formation of a dinuclear system contribute to the quasifission and complete-fusion processes in massive nuclei reactions at different energies of CN. We found that the competition between quasifission and fusion starts from low values (at about $L = 6$–$8\hbar$) of the initial orbital angular momentum. The contribution of quasifission increases with L, and it is larger for the reaction induced by a heavier ion beam. Effects of the entrance channel become apparent in a number of partial waves leading to capture and complete fusion. The number of partial waves ℓ contributing to capture is determined by the size of the well in the nucleus-nucleus potential and the moment of inertia which are different for the ^{16}O + ^{204}Pb and ^{96}Zr + ^{124}Sn reactions due to difference in their mass and charge asymmetries. The number of partial waves leading to complete fusion depends on the height of the quasifission ($B_{\rm qf}$) and intrinsic fusion ($B^*_{\rm fus}$) barriers which are different in these reactions. Such a difference of the entrance channel affects the compound nucleus formation and the real fission probability of CN, at lower and higher excitation energy values and for each orbital angular-momentum value. The study of the dependence of the nucleus fission probability on the entrance channel showed that there is a large difference between fission probabilities of the excited compound nucleus formed in these reactions at $E^* < 45$ MeV. Due to the large moment of inertia of the dinuclear system formed in the ^{96}Zr + ^{124}Sn reaction, large values of the angular momentum contribute to capture and fusion. But the fission barrier decreases with increasing L: as parameterized by Sierk [20] for the macroscopic part, and by the factor $q(L)$ which damps the shell correction to the fission barrier (see eqs. (7) and (8)) for the microscopic part. Instead, the small moment of inertia of the dinuclear system formed in the ^{16}O + ^{204}Pb reaction does not allow capture and fusion at high angular-momentum values for beam energies close to the Coulomb barrier. The decisive role of the value $E^* = 45$ MeV for the ^{16}O + ^{204}Pb reaction is connected with the fact that this value corresponds to the formation of the compound nucleus with an angular momentum at which shell corrections to the fission barrier disappear.

We presented a detailed description on the angular-momentum values of the intermediate excited nuclei formed along the de-excitation cascade of CN after neutron emission and showed how the evaporation residue cross-section changes at different excitation energy E^* for the two reactions. We also revealed the role of different trends of fission probability of excited nuclei for each step of the de-excitation cascade, and we found that fission probability increases for the subsequent excited nuclei formed along the CN cascade.

We found that the ER formation is mainly affected by the first steps of the de-excitation cascade of CN. At a higher excitation energy E^*, the fission probability of such excited nuclei is comparable for the corresponding steps of the cascade of CN produced in two reactions. At lower excitation energies, the fission probability at various steps is much higher for the de-excitation cascade of CN obtained in the more symmetric reaction.

A.K.N. is grateful to STCU (Grant Uzb-45, Kiev), RFBR 02-02-04013 (Moscow) and the JINR-Polish Agreement for financial support. A.K.N. also thanks the University of Messina and the FBP of Messina for the hospitality and the appreciable support during his stay in Messina.

References

1. D.J. Hinde, M. Dasgupta, A. Mukherjee, Phys. Rev. Lett. **89**, 282701 (2002).
2. A.C. Berriman *et al.*, Nature (London) **413**, 144 (2001).
3. C.-C. Sahm, H.-G. Clerc, K.-H. Schmidt, W. Reisdorf, P. Armbruster, F.P. Heßberger, J.G. Keller, G. Münzenberg, D. Vermeulen, Nucl. Phys. A **441**, 316 (1985).
4. B.B. Back, P.B. Fernandez, B.G. Glagola, D. Henderson, S. Kaufman, J.G. Keller, S.J. Sanders, F. Videbæk, T.F. Wang, B.D. Wilkins, Phys. Rev. C **53**, 1734 (1996).
5. S. Mitsuoka, H. Ikezoe, K. Nishio, J. Lu, Phys. Rev. C **62**, 054603 (2000).
6. G. Giardina, F. Hanappe, A.I. Muminov, A.K. Nasirov, L. Stuttgé, Nucl. Phys. A **671**, 165 (2000).

7. G. Giardina, S. Hofmann, A.I. Muminov, A.K. Nasirov, Eur. Phys. J. A **8**, 205 (2000).
8. G. Fazio, G. Giardina, A. Lamberto, R. Ruggeri, C. Saccà, R. Palamara, A.I. Muminov, A.K. Nasirov, U.T. Yakhshiev, F. Hanappe, T. Materna, L. Stuttgé, Eur. Phys. J. A **19**, 89 (2004).
9. G. Fazio, G. Giardina, A. Lamberto, R. Ruggeri, C. Saccà, R. Palamara, A.I. Muminov, A.K. Nasirov, U.T. Yakhshiev, F. Hanappe, T. Materna, L. Stuttgé, J. Phys. Soc. Jpn. **72**, 2509 (2003).
10. V.V. Volkov, N.V. Antonenko, E.A. Cherepanov, A.K. Nasirov, V.P. Permjakov, Phys. Lett. B **319**, 425 (1993); Phys. Rev. C **51**, 2635 (1995).
11. D.H.E. Gross, R.C. Nayak, L. Satpathy, Z. Phys. A **299**, 63 (1981).
12. P. Fröbrich, Phys. Rep. **116**, 337 (1984); Phys. Lett. B **215**, 36 (1988).
13. A. D'Arrigo, G. Giardina, M. Herman, A. Taccone, Phys. Rev. C **46**, 1437 (1992).
14. A. D'Arrigo, G. Giardina, M. Herman, A.V. Ignatyuk, A. Taccone, J. Phys. G **20**, 365 (1994).
15. R.N. Sagaidak, V.I Chepigin, A.P. Kabachenko, J. Roháč, Yu.Ts. Oganessian, A.G. Popeko, A.V. Yeremin, A. D'Arrigo, G. Fazio, G. Giardina, M. Herman, R. Ruggeri, R. Sturiale, J. Phys. G **24**, 611 (1998).
16. G. Audi, A.H. Wapstra, Nucl. Phys. A **595**, 509 (1995).
17. P. Möller, J.R. Nix, At. Data Nucl. Data Tables **39**, 213 (1988).
18. S. Raman, C.H. Malarkey, W.T. Milner, C.W. Nestor jr., P.H. Stelson, At. Data Nucl. Data Tables **36**, 1 (1987).
19. R. H. Spear, At. Data Nucl. Data Tables **42**, 55 (1989).
20. A.J. Sierk, Phys. Rev. C **33**, 2039 (1986).